Fabrication of Large-Area Bimodal Sensors by All-Inkjet-Printing

Sheng Fu, Juan Tao, Wenqiang Wu, Junlu Sun, Fangtao Li, Jing Li, Zhihao Huo, Zhiguo Xia, Rongrong Bao,* and Caofeng Pan**

Electronic skin (e-skin) is a wearable smart terminal that senses changes of external environment like human skin. It will develop into an indispensable way of interaction between humanity and technology. Here, this bimodal e-skin that senses bending strain and pressure using an all-inkjet-printing method is synthesized. It is based on a microcracked metal film and a sandwich capacitor structure. It is characterized by the metal film of the strain sensor as a bottom electrode of pressure sensor; the electrode plate of the device plays a dual role. When tested, the strain sensor and pressure sensor do not interfere with each other. The device has excellent performance with low pressure-detection of 2 Pa and high stability over more than 5700 cycles for pressure sensor and high gauge factor (4000) and good stability (over 4500 cycles) for strain sensor, which can recognize the radius of curvature of human activities and objects, and can detect the pressure distribution and the curvature of irregular surfaces, showing its potential applications in wearable devices.

1. Introduction

E-skin has recently attracted significant attention due to their facile interaction with human body and simple structure.[1] It emulates human skin to detect temperature,[2] strain,[3–9] humidity,[10] and pressure[11–15] by converting external stimuli into electrical signals. Improving the performance of electronic skin (e-skin) and adding more features is its development goal. With the development of technology, e-skin will eventually become an important way for us to accurately sense various external stimuli.

In terms of performance, for e-skin that can sense strain, researchers often use rigid conductive materials to construct new structures, such as graphene,[16] carbon nanotubes,[17,18] and carbons,[19] but their sensitivity is generally low, while microcrack-based metal film strain sensors have good performance[5]; for e-skins that can sense pressure, capacitive pressure sensors have the advantage of simple structure. In this respect, it is better than piezoelectricity[20,21] and piezoresistivity.[22,23] In terms of functionality, recently researches reported the e-skin to be no longer limited to the function of human skin; it has been successfully expanded to sense light, magnetic field, and proximity.[24]

In practical applications, human skin is subjected to different external stimuli simultaneously. This means that the e-skin must be designed to allow multiple modes to sense multiple stimuli in order to better mimic human skin.[10] Achieving this goal requires a single point of multilayer device fabrication.[25] So far, several approaches have been reported to simultaneously measure pressure and other physical quantities, such as temperature[26–28] or humidity[10] simultaneously. However, there are still some problems as follows: 1) more material waste,[29] 2) not environmentally friendly, 3) sophisticated fabrication processes including photolithography, vacuum deposition, and electroless plating processes;[30] these operations are very complicated, 4) difficult to commercialize.

In this condition, we need a high-efficient, eco-friendly, cost-saving manufacture technology; one of the most promising alternatives is the inkjet printing. Inkjet printing is a material-conserving deposition technique used for liquid phase materials.[31] Inkjet printing has many other advantages, such as mask-free, cost-effective, and non-toxic. Materials

S. Fu, J. Tao, W. Q. Wu, J. L. Sun, J. Li, Z. H. Huo, Prof. R. R. Bao, Prof. C. F. Pan
CAS Center for Excellence in Nanoscience
Beijing Key Laboratory of Micro-nano Energy and Sensor
Beijing Institute of Nanoenergy and Nanosystems
Chinese Academy of Sciences
Beijing 100083, P. R. China
E-mail: Baorongrong@binn.cas.cn; cfpan@binn.cas.cn

S. Fu, F. T. Li, Prof. Z. G. Xia
The Beijing Municipal Key Laboratory of New Energy Materials and Technologies
School of Materials Sciences and Engineering
University of Science and Technology Beijing
Beijing 100083, P. R. China
E-mail: xiazg@ustb.edu.cn

J. Tao, J. Li, Z. H. Huo, Prof. R. R. Bao, Prof. C. F. Pan
School of Nanoscience and Technology
University of Chinese Academy of Sciences
Beijing 100049, P. R. China

Prof. R. R. Bao, Prof. C. F. Pan
Center on Nanoenergy Research
School of Physical Science and Technology
Guangxi University
Nanning, Guangxi 530004, P. R. China

Prof. C. F. Pan
College of Optoelectronic Engineering
Shenzhen University
Shenzhen 518060, China

The ORCID identification number(s) for the author(s) of this article can be found under https://doi.org/10.1002/admt.201800703.

DOI: 10.1002/admt.201800703

for inkjet printing are extensive: organic[32,33] and inorganic[34,35] conducting, semiconducting,[36] and dielectric materials can be used as ink for printing. Ink can be printed on a variety of substrates like paper,[37] polymer,[38] textile,[39] plastic,[33] and glass.[39] With this patterning methodology and proper inks, various types of sensors have been prepared by inkjet printing, such as biosensor for detecting several analytes,[40] touch sensing device,[41]strain sensor,[42] humidity sensor,[43] pressure, and temperature bimodal sensor,[28]

Here, we use an all-inkjet-printing method to prepare such a bimodal sensor that can simultaneously sense bending strain and pressure. Silver nanoparticles (AgNPs) suspension was used as the conductive ink. The sensor unit is composed of a bottom electrode on polyethylene naphthalate (PEN) and a top electrode on paper. The bottom electrode serves as a strain sensor based on micro crack; it combines with the top electrode to form capacitive pressure sensor. The resulting pressure sensor exhibited high sensitivity, low pressure-detection of 2 Pa, wide range of pressure sensing, and fast response time of 126 ms, high stability more than 5700 cycles. At the same time, the strain sensor had high sensitivity, fast response (154 ms), good stability (over 4500 cycles), and high gauge factor (4000). The gauge factor refers to the relative change in resistance and corresponding mechanical strain ratio. Furthermore, we demonstrated 16 pixels pressure sensor arrays and quadrangular strain arrays which can sense pressure and strain distribution.

2. Results and Discussion

The body's skin is a huge sensory system that can detect external pressure on it and its own bending, and then pass through the neurons to the body's processing system—the brain (see **Figure 1**a). As shown in Figure 1b, we demonstrate an all-inkjet-printing approach for fabricating flexible pressure and strain bimodal sensor to simulate this sensing process. The device implements a single point dual function sensing. The diagram in blue dashed line is the principle of its test; LCR meter and computer serves as processing system of our simulation system.

Figure 2a presents the fabrication procedure of bimodal sensor. We used PEN with thickness of 125 μm as the substrate due to its good flexibility and hydrophilicity; so, the devices can be flexible and the PEN was printed with AgNPs directly which did not require hydrophilic treatment. AgNPs suspension was printed on a cleaned PEN film and was sintered at 100 °C for 2 min to enhance its conductance and decrease drying time; sintering leads to enhance particle network densification;[44] too dense metal film is not conducive to be strain sensor. The thickness of metal film on PEN is 3.3 μm (see Figure 2e). After the Ecoflex was coated onto the substrate as a dielectric layer, a piece of paper was tiled on it. The paper can be firmly attached to it due to the high viscosity of Ecoflex surface. Finally, a top electrode was printed on paper and the device was encapsulated by Ecoflex (see thickness of each layer in Figure S1, Supporting

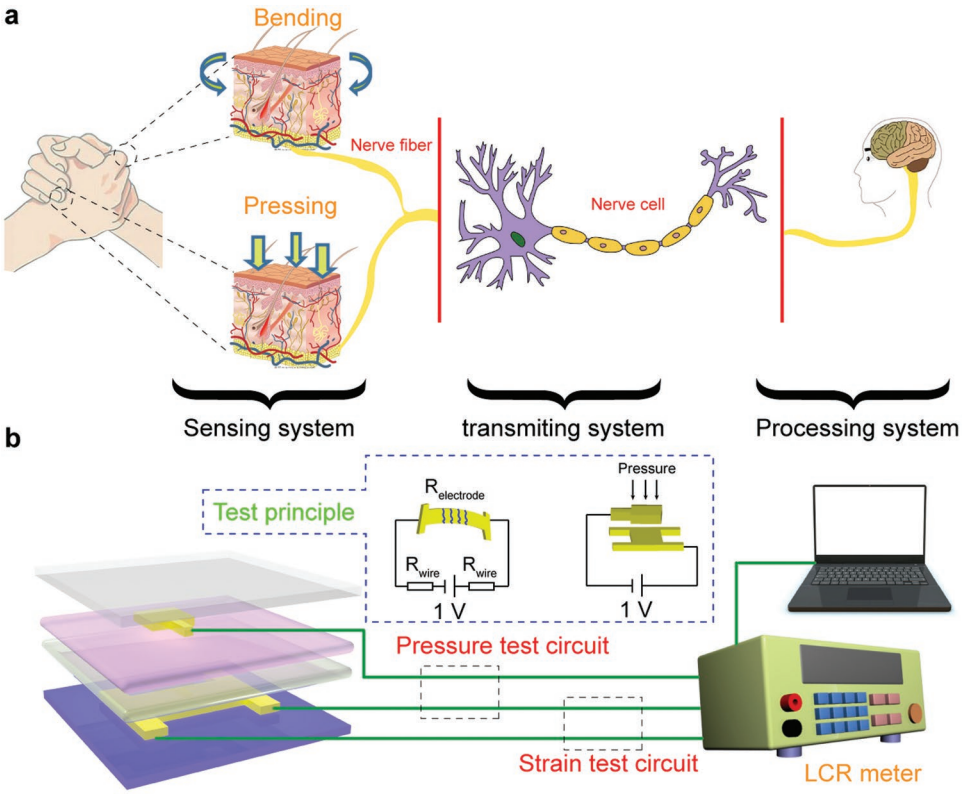

Figure 1. Human body sensing system and simulation. a) Processing of human body senses pressure and bending. b) Simulation of human skin sensing process.

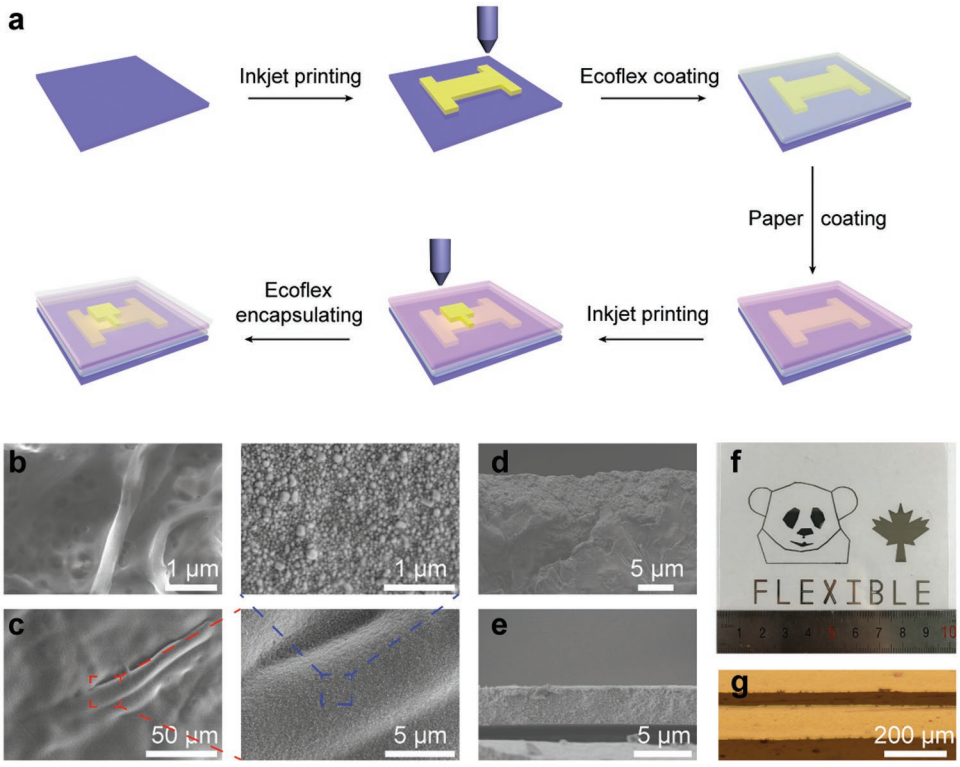

Figure 2. The fabrication of bimodal sensor. a) Schematic illustration of the fabrication of bimodal sensor and circuit diagram. b) SEM image of the morphology of paper surface. c) SEM image of AgNPs coating on the paper at different magnification. d,e) SEM images of the cross section of paper and PEN covered by AgNPs, respectively. f) Different conductive drawings printed on PEN. g) Line spacing and width.

Information). The effective length of bottom electrode is 10 mm, and the effective area of top electrode is 9 mm^2 (see Figure S2, Supporting Information). The reason of choosing such a size is shown in Figure S3 in the Supporting Information.

The pan paper we used was soaked in glycerinum, so, the ink will not spread when printed on it. The paper is a porous structure (see Figure 2b); silver ink will penetrate into the paper and the internal AgNPs can be observed (see Figure 2d). Figure 2c shows the top view scanning electron microscopy (SEM) images of paper covered with AgNPs at different magnifications, showing that the surface of paper is completely covered by AgNPs and the AgNPs coating is uniform. The paper electrode was bent by a linear motor for 900 cycles to confirm the durability and flexibility. Due to the good performance of paper, the resistance of the conductive paper shows no obvious degradation (see Figure S4, Supporting Information). The top electrode is printed on the paper layer. Soft and porous structure of paper can avoid cracks and maintainthe effective area of the electrode during the bending process. The thickness of metal film above paper is about 2.7 μm; this result is calculated based on the average thickness (see Figure 2d).Various patterns and letters were successfully fabricated on PEN without mask (see Figure 2f); this fully proves the flexibility of inkjet printing. Figure 2g shows that the smallest line spacing and width are 66 and 155 μm, respectively.

2.1. Characterization of Strain Sensor

The bimodal sensor is flexible as the PEN and paper are very thin. Before the device is used, we need to pre-bend the device. Some cracked channels which perpendicular to the direction of pre-bend appeared had been caused by Poisson effect. And most of them stray closed after the strain disappearwith the overlapped crack edges. Therefore, the working principle of the sensor can be interpreted as overlap mode and tunnel effect[5] (see Figure S5, Supporting Information). Applying an external strain would change the state of cracks; as a result, the output current changes. Calculation of bending strain is shown in Figure S6 in the Supporting Information. What needs to be emphasized is that the strain sensor can act as a bottom electrode, cooperating with the top electrode to form capacitive pressure sensor. The variation of capacitance is responsible for the sensor's response to the applied external pressure.

Here, we use custom-built sensor probe station to characterize electromechanical capability of the strain sensor; a liner motor is used to apply strains and LCR meter measure the change of resistance (see Figure S7, Supporting Information). **Figure 3**a shows the deformation state of the device when tested for strain. It should be noted that the top electrode is facing the endpoint of effective area of the bottom electrode, as shown in Figure 3b. 0.52% strain was used to bend the device, the resistance of the strain sensor has changed, and the capacitance of pressure has a negligible response. This proves that the two sensors do not interfere with each other.

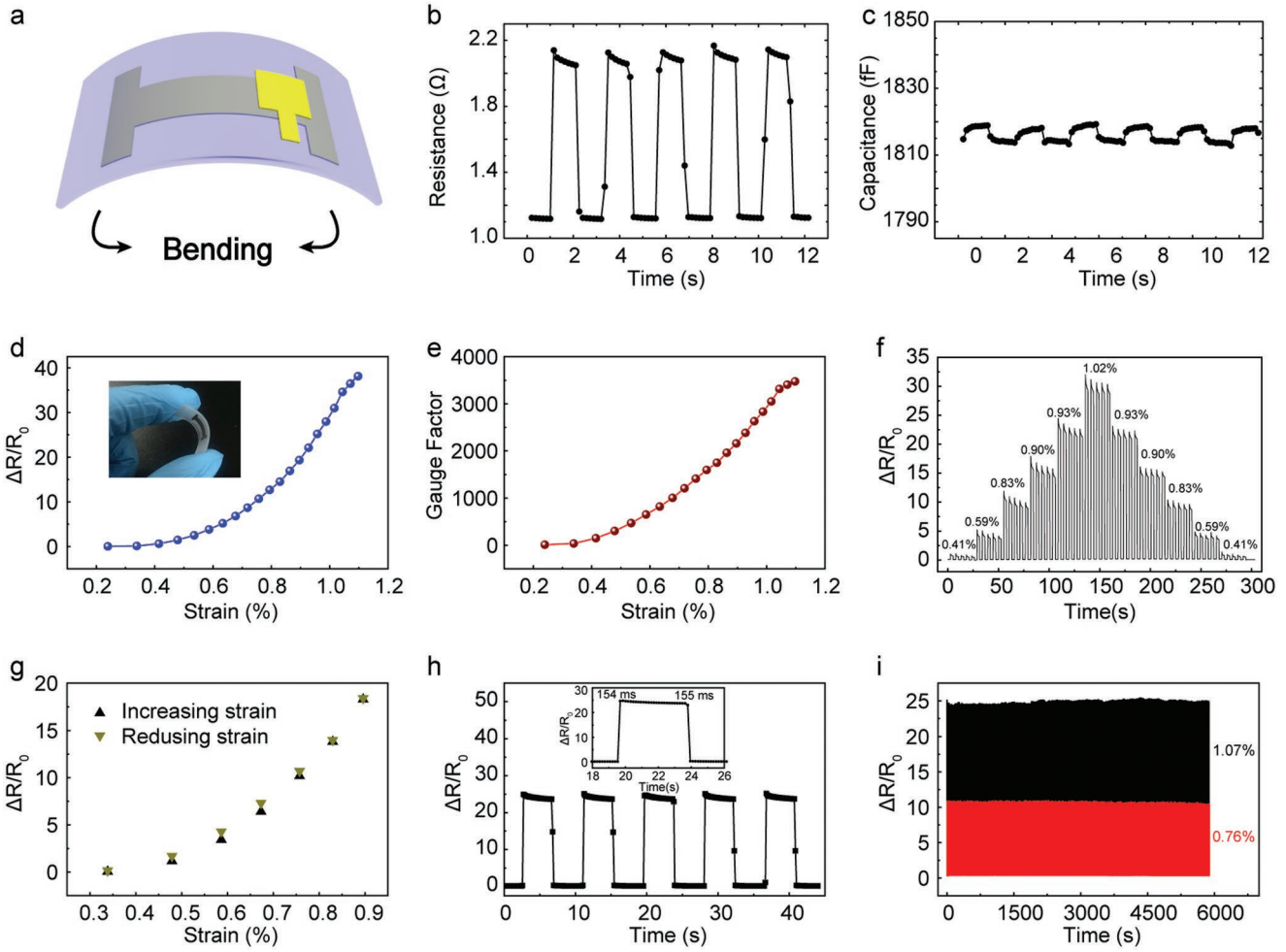

Figure 3. Electromechanical capability of the strain sensor. a) Schematic diagram of the strain exerted on the device. b,c) The change of resistance and capacitance when 0.52% strain was used to bend the device. d) Relative resistance changes of the strain sensor with a rising strain. e) Gauge factor of the strain sensor under different strains. f,g) The resistance of the strain sensor under increasing and reducing strains. h) Time response of the strain sensor. Inset shows the response times of 154 and 155 ms for rising and recovering, respectively. i) Mechanical durability of the strain sensor under a strain of 0.76% and 1.07%, respectively.

The strain sensing capability of the bimodal sensor was explored by applying bending force to the sensing cell. Figure 3d shows the relative resistance change ($\Delta R/R_0$) of the strain sensor at different strains. The minimum measurement limit of strain is about 0.21%, because the bottom electrode we prepared is thick, and the small strain does not cause cracks. At the beginning, the relative resistance change increases slowly; after 4% strain the curve becomes sharp with the increasing strain. This phenomenon can be perfectly explained by the proposed working mechanism. The gauge factor (**GF**) is an important index to evaluate the performance of the strain sensor, and is defined as $\mathbf{GF} = (\Delta R/R_0)/\varepsilon$ (ε is the mechanical strain); the highest GF value of our strain sensor is about 3500 (see Figure 3e), which is better than most strain sensor based on graphite,[45] nanowires.[46] As shown in Figure 3f, the stepped strain is applied to the strain sensor to study its reproducibility. The result indicates the sensor have good reproducibility at the wide range of 0.41–1.10%. Figure 3f,g shows that the sensor has negligible hysteresis, when the strain is increased, the device generates new cracks. When the strain is gradually reduced, the same strain resistance will increase slightly due to the new crack. Figure 3h shows the strain sensor process five cycles at 0.93% strain and the inset view shows that the response and relaxation times of the sensor is 154 and 155 ms, respectively. This strain sensor shows good stability by repeatedly load/unload strain of 0.76% and 1.07% for about 4500 cycles without obviously degradation of the sensing performance (see Figure 3i).

2.2. Characterization of Pressure Sensor

Similar to Figure 3a, the performance of the bimodal sensor capability as a pressure sensor was investigated by using a custom-built sensor probe station (see Figure S7, Supporting Information). **Figure 4**a shows device deformation when pressure is applied. As shown in Figure 4b,c, when

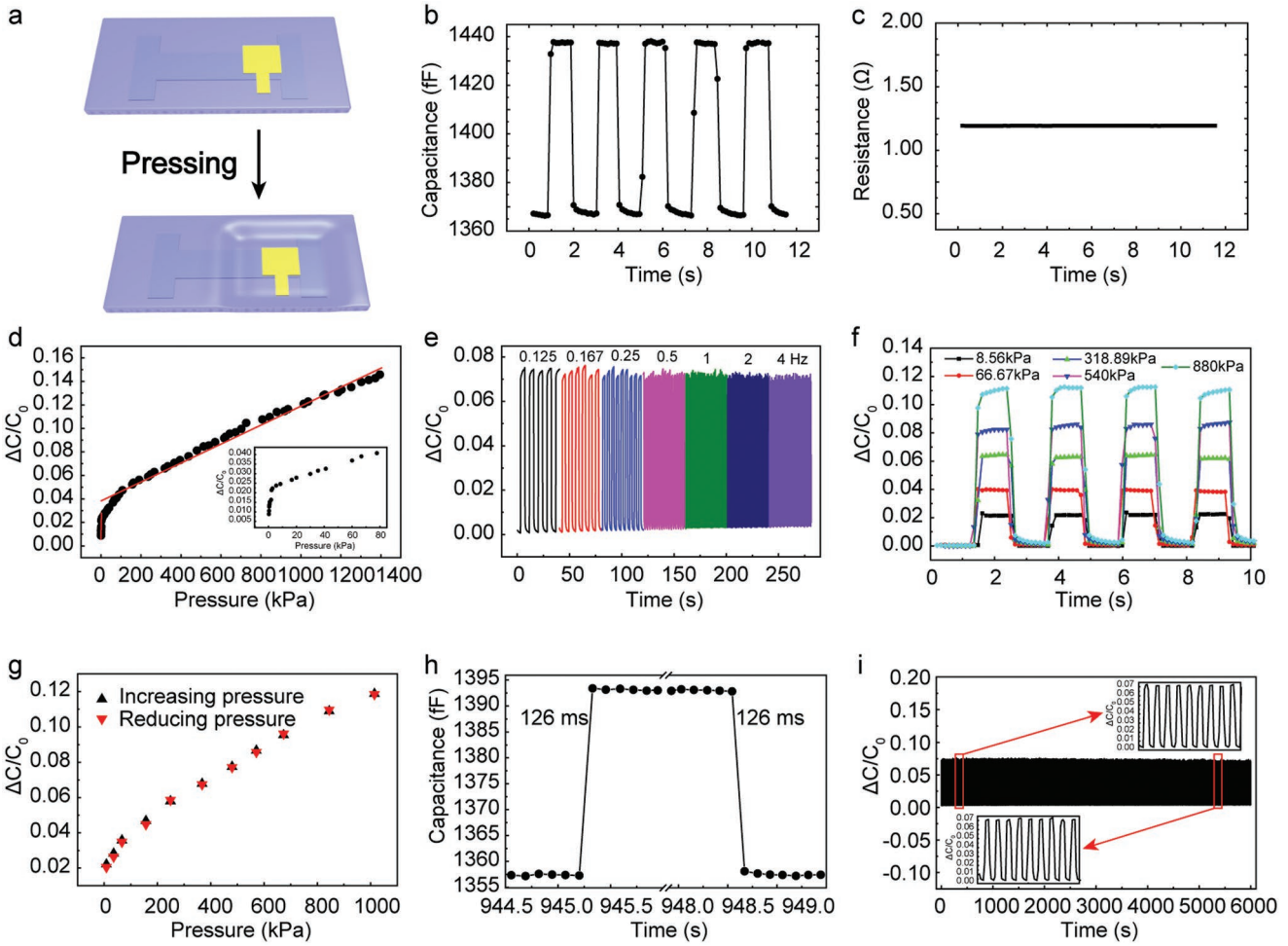

Figure 4. Pressure sensing capability of the bimodal sensor. a) Schematic diagram of pressing the device. b,c) Two signal responses when pressure of 202.8 kPa applied to the bimodal sensor. d) Relative capacitance change ($\Delta C/C_0$) of the pressure sensor versus pressure. e) Relative capacitance response of the pressure sensor as a function of the loading frequency at a pressure of 202.8 kPa. f) $\Delta C/C_0$ versus time four cycles of five different applied pressure. g) The reversible capacitance changes of the pressure sensor under increasing and reducing pressure. h) Response and delay time of the pressure sensor. i) The durability test of our pressure sensor under a pressure of 202.8 kPa.

a pressure applied to the bimodal sensor, pressure sensor has a clear response and the resistance of the strain has no obvious change. The performance of the bimodal sensor capability used as a pressure was investigated. Figure 4d plots the relative capacitance change under different pressure loading; the curve shows a quasi-bilinear character, which is due to incompressibility of the Ecoflex dielectric.[10] Initially, the dielectric layer is easily compressed, and as the thickness of the dielectric layer decreases, a greater force is necessarily applied to reduce the same thickness. In order to evaluate the performance of our device, here, the sensitivity S of the pressure sensor was introduced, which defined as the slope of the curve, as given by equation $S = (\Delta C/C_0)/\Delta P$ (C_0 defined as the original capacitance of the device, ΔC is the change of capacitance, ΔP being the change in applied pressures).[47] For pressures below 2.9 kPa and above 2.9 kPa, the sensitivity of the pressure sensor is 0.0049 kPa^{-1} and 0.081 MPa^{-1}, respectively. In practical applications, frequency-dependence of pressure sensor is one of the major characteristics. Figure 4e shows the relative capacitance change of the pressure sensor at different frequencies with a pressure of 202.8 kPa, the base value has a slight increase; this result is attributed to the viscoelasticity of the Ecoflex dielectric layer; as the frequency increases, the dielectric layer does not return to the initial state within a gradually shortened time. Frequency of 4 Hz is enough to meet practical application. Figure 4f shows representative capacitance profiles ($\Delta C/C_0$) of the pressure sensor at five different pressures. As shown in Figure 4g, increasing and reducing pressure are applied to the pressure sensor; it can be seen that the two sets of experimental data are almost completely coincident, which indicates that our device has good reversibility. Response and delay time of the pressure sensor is 126 and 126 ms, respectively. After 6000 s (about 5700 cycles) repeated loading-unloading cycling tests, no degradation can be found in Figure 4i, which indicates our device have credible stability and durability.

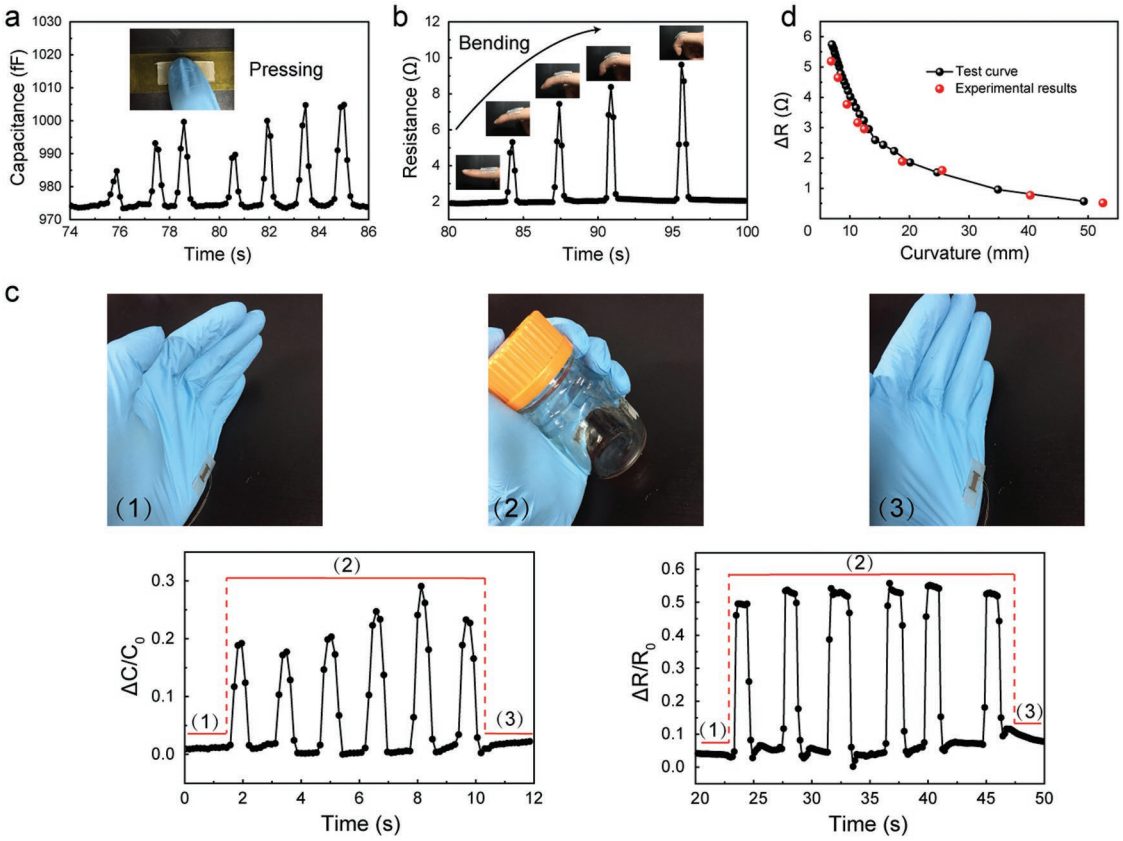

Figure 5. Detection of different human motion and application of the bimodal sensor. a) Optical images and corresponding capacitance signal of the bimodal sensor when pressing the device. b) Photograph images and related current signal of the device when attaching the device on a bent finger. c) Detecting the process of grasping an object and corresponding two different signals. d) Resistance change versus curvature curve of the bimodal sensor and measured data of nine objects with different curvature.

2.3. Application of the Bimodal Sensor

Due to high flexibility and excellent performance of the bimodal sensor, we use this device to detect human motion and explore its practical applications. **Figure 5**a shows capacitance responses to different pressure, indicating that our device can accurately detect the magnitude of external force in real time. Our device can be attached to the joint of the finger to detect the bending of the finger; the greater the degree of bending the greater the corresponding resistance (see Figure 5b).

Strain and pressure sensors can work together (see Figure 5c). The device is attached to the lower part of the palm; when the hand to grasp the jar, due to the palm and the object's squeeze, pressure sensor produces a change in capacitance, and the bending of the palm will cause the strain sensor to produce a resistance response. As expected, with different squeeze pressures, the response of the pressure sensor will be different. Since the radius of curvature of the jar is constant, the grip strength does not affect the degree of response of the strain sensor. The pressure measurement limit of this device is 2 Pa (see Figure S8, Supporting Information). Due to the high sensitivity and stability of the two sensors, our device can be mounted on the hand, and when gripping an object, the magnitude of the force and the curvature of the object can be perceived. Figure 5d indicates the actual measurement of objects with different curvatures and experimental curve are almost completely coincident.

3. Array Sensor of the Device

Here, we built a bimodal sensors array to spatially map strain and pressure distribution. As shown in **Figure 6**a, the sensing array contains 4×4 pixels; maskless inkjet printing method was used to print designed bottom strain sensor and top electrodes; the other steps are the same as for making a single device. Figure 6b shows this array is attached to the back of the hand to measure the strain distribution of the device. From Figure 6c we can see that the strain distribution is in line with the bending of the opisthenar. Since the lower half of the back of the hand is narrower, the lower left corner of the array device mainly measures the bending of the wrist, which is the most curved.

Accurate pressure distribution can be achieved here. As shown in Figure 6d, the array can accurately identify the position of the acrylic cylinder. Next, different numbers of cylinders are randomly distributed on the device; its number and position can be correctly identified (see Figure 6e–h). When N-shaped

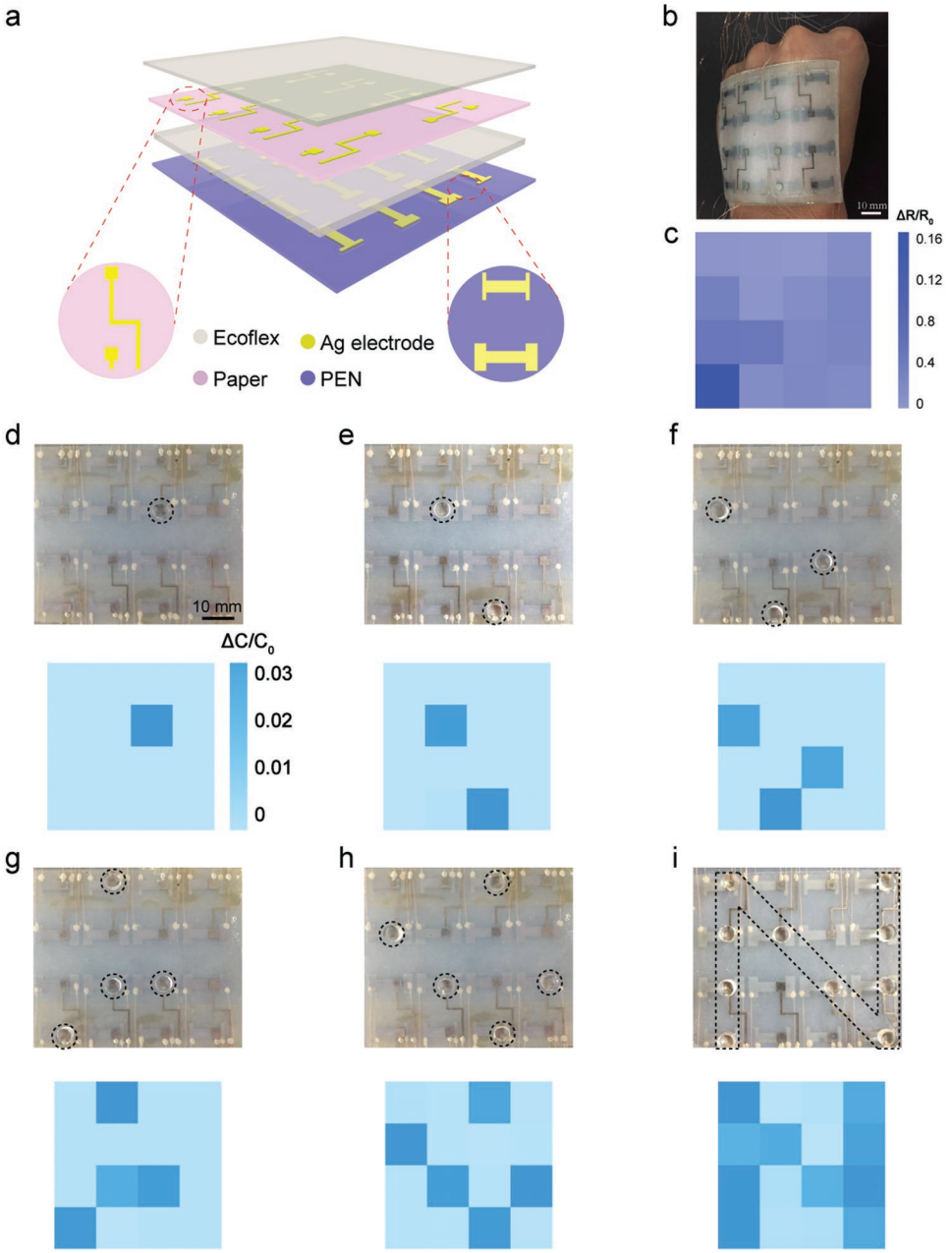

Figure 6. Detection of stain and pressure distribution by the strain sensor array. a) Schematic view of the bimodal sensor array with 4 × 4 pixels. b) Photograph of strain sensor array is attached to the back of the hand. c) The corresponding mapping of strain distribution. d–h) Photographs of the sensing array with increasing number of acrylic cylinder and corresponding mappings of the pressure distribution. i) A photograph of the sensor array pressed by 10 cylinders with N-shaped and the corresponding capacitance signals of the 16 pixels.

acrylic cylinders were placed on the pressure sensor arrays (Figure 6i) the output signal literally represents the shape of the placed object.

4. Conclusion

In conclusion, we report an all-inkjet-printing approach for fabricating flexible bimodal sensor and large-area sensing arrays. The sensor can simultaneously detect external pressure and strain stimuli. The device has excellent performance with low pressure-detection of 2 Pa and high stability over more than 5700 cycles for pressure sensor and high gauge factor (4000) and good stability (over 4500 cycles) for strain sensor. The devices can monitor human activities like human skin, and even real-time-readable measuring the pressure of the contacted object and its curvature. Subsequently, pressure and strain distribution is achieved using the multipixel sensor arrays. Based on inkjet-printing, the work is expected as a foreshadowing to create simple and multimodel e-skin.

5. Experimental Section

Fabrication of Strain Sensors: PEN with a protective film on both sides, did not require further cleaning. Subsequently, it was fixed on a glass substrate. Then, a silver metal layer was deposited on the PEN substrate via the inkjet printer (SonoPlot).Finally it was baked at 100 °C for 5 min.

Fabrication of the Bimodal Sensor: On the basis of the previous step, a layer of Ecoflex was covered onto strain sensor which was prepared by solidifying the mixture of the A and B with a weight ratio of 1:1 at 70 °C for 10 min. Subsequently, a piece of paper was tiled on top of Ecoflex and placed in a vacuum oven to remove air bubbles. Then, the ink was printed on paper and dried. Finally, the sensor was encapsulated with Ecoflex.

Fabrication of Multipixel Sensor Array: The first layer of metal thin film with the design pattern was firstly printed on the PEN substrate by inkjet printer. Subsequently, the second layer of Ecoflex and the third layer of paper were deposited on the first. Finally, the 4 × 4 pixel arrays were printed on paper to form large-area, patterned bimodal sensors.

Characterization: A LabVIEW controlled digital source meter (Keithley 2450) was used to measure the *I–t* and *C–t* curves in real-time. The SEM images were collected using a Hitachi SU8200. A step motor (LinMot E1100) was used to test the mechanical stability of the device.

Supporting Information

Supporting Information is available from the Wiley Online Library or from the author.

Acknowledgements

The authors thank the support of national key R & D project from Minister of Science and Technology, China (2016YFA0202703), National Natural Science Foundation of China (No. 51622205, 61675027, 51432005, 61505010, and 51502018), Beijing City Committee of science and technology (Z171100002017019 and Z181100004418004), and Beijing Natural Science Foundation (4181004, 4182080, 4184110, and 2184131).

Conflict of Interest

The authors declare no conflict of interest.

Keywords

arrays, bimodal sensors, inkjet printing, pressure sensors, strain sensors

Received: December 13, 2018
Revised: January 15, 2019
Published online:

[1] M. Amjadi, K.-U. Kyung, I. Park, M. Sitti, *Adv. Funct. Mater.* **2016**, *26*, 1678.
[2] Y. Chen, B. Lu, Y. Chen, X. Feng, *Sci. Rep.* **2015**, *5*, 11505.
[3] C. Pang, G. Y. Lee, T. I. Kim, S. M. Kim, H. N. Kim, S. H. Ahn, K. Y. Suh, *Nat. Mater.* **2012**, *11*, 795.
[4] Y. Wang, L. Wang, T. Yang, X. Li, X. Zang, M. Zhu, K. Wang, D. Wu, H. Zhu, *Adv. Funct. Mater.* **2014**, *24*, 4666.
[5] C. Wang, J. Zhao, C. Ma, J. Sun, L. Tian, X. Li, F. Li, X. Han, C. Liu, C. Shen, L. Dong, J. Yang, C. Pan, *Nano Energy* **2017**, *34*, 578.
[6] X. Wang, Y. Zhang, X. Zhang, Z. Huo, X. Li, M. Que, Z. Peng, H. Wang, C. Pan, *Adv. Mater.* **2018**, *30*, 1706738.
[7] M. Su, F. Li, S. Chen, Z. Huang, M. Qin, W. Li, X. Zhang, Y. Song, *Adv. Mater.* **2016**, *28*, 1369.
[8] M. Su, Z. Huang, F. Li, Z. Zhang, Y. Guo, Z. Cai, Y. Li, W. Li, X. Qian, Y. Li, X. Zhang, Y. Song, *Adv. Mater. Technol.* **2018**, *3*, 1800107.
[9] Y. Li, Y. Li, M. Su, W. Li, Y. Li, H. Li, X. Qian, X. Zhang, F. Li, Y. Song, *Adv. Electron. Mater.* **2017**, *3*, 1700253.
[10] S. Y. Kim, S. Park, H. W. Park, D. H. Park, Y. Jeong, D. H. Kim, *Adv. Mater.* **2015**, *27*, 4178.
[11] Q. Shao, Z. Niu, M. Hirtz, L. Jiang, Y. Liu, Z. Wang, X. Chen, *Small* **2014**, *10*, 1466.
[12] C. L. Choong, M. B. Shim, B. S. Lee, S. Jeon, D. S. Ko, T. H. Kang, J. Bae, S. H. Lee, K. E. Byun, J. Im, Y. J. Jeong, C. E. Park, J. J. Park, U. I. Chung, *Adv. Mater.* **2014**, *26*, 3451.
[13] Q. Sun, D. H. Kim, S. S. Park, N. Y. Lee, Y. Zhang, J. H. Lee, K. Cho, J. H. Cho, *Adv. Mater.* **2014**, *26*, 4735.
[14] Y. Joo, J. Byun, N. Seong, J. Ha, H. Kim, S. Kim, T. Kim, H. Im, D. Kim, Y. Hong, *Nanoscale* **2015**, *7*, 6208.
[15] R. Bao, C. Wang, L. Dong, C. Shen, K. Zhao, C. Pan, *Nanoscale* **2016**, *8*, 8078.
[16] A. V. Zaretski, S. E. Root, A. Savchenko, E. Molokanova, A. D. Printz, L. Jibril, G. Arya, M. Mercola, D. J. Lipomi, *Nano Lett.* **2016**, *16*, 1375.
[17] T. Yamada, Y. Hayamizu, Y. Yamamoto, Y. Yomogida, A. Izadi-Najafabadi, D. N. Futaba, K. Hata, *Nat. Nanotechnol.* **2011**, *6*, 296.
[18] N. Lu, C. Lu, S. Yang, J. Rogers, *Adv. Funct. Mater.* **2012**, *22*, 4044.
[19] J.-H. Kong, N.-S. Jang, S.-H. Kim, J.-M. Kim, *Carbon* **2014**, *77*, 199.
[20] R. Bao, C. Wang, L. Dong, R. Yu, K. Zhao, Z. L. Wang, C. Pan, *Adv. Funct. Mater.* **2015**, *25*, 2884.
[21] C. Wang, R. Bao, K. Zhao, T. Zhang, L. Dong, C. Pan, *Nano Energy* **2015**, *14*, 364.
[22] L. Pan, A. Chortos, G. Yu, Y. Wang, S. Isaacson, R. Allen, Y. Shi, R. Dauskardt, Z. Bao, *Nat. Commun.* **2014**, *5*, 3002.
[23] L. W. Yap, S. Gong, Y. Tang, Y. Zhu, W. Cheng, *Sci. Bull.* **2016**, *61*, 1624.
[24] Q. Hua, J. Sun, H. Liu, R. Bao, R. Yu, J. Zhai, C. Pan, Z. L. Wang, *Nat. Commun.* **2018**, *9*, 244.
[25] D. Tang, Q. Wang, Z. Wang, Q. Liu, B. Zhang, D. He, Z. Wu, S. Mu, *Sci. Bull.* **2018**, *63*, 574.
[26] N. T. Tien, S. Jeon, D. I. Kim, T. Q. Trung, M. Jang, B. U. Hwang, K. E. Byun, J. Bae, E. Lee, J. B. Tok, Z. Bao, N. E. Lee, J. J. Park, *Adv. Mater.* **2014**, *26*, 796.
[27] C. Hou, H. Wang, Q. Zhang, Y. Li, M. Zhu, *Adv. Mater.* **2014**, *26*, 5018.
[28] K. Kim, M. Jung, B. Kim, J. Kim, K. Shin, O.-S. Kwon, S. Jeon, *Nano Energy* **2017**, *41*, 301.
[29] X. Wang, J. Hao, *Sci. Bull.* **2016**, *61*, 1281.
[30] M. Stoppa, A. Chiolerio, *Sensors* **2014**, *14*, 11957.
[31] M. Singh, H. M. Haverinen, P. Dhagat, G. E. Jabbour, *Adv. Mater.* **2010**, *22*, 673.
[32] K. S. Park, J. Baek, Y. Park, L. Lee, Y. E. Lee, Y. Kang, M. M. Sung, *Adv. Mater.* **2016**, *28*, 2874.
[33] J. L. Zhuang, D. Ar, X. J. Yu, J. X. Liu, A. Terfort, *Adv. Mater.* **2013**, *25*, 4631.
[34] X. Wang, H. Hu, Y. Shen, X. Zhou, Z. Zheng, *Adv. Mater.* **2011**, *23*, 3090.
[35] J. Li, F. Ye, S. Vaziri, M. Muhammed, M. C. Lemme, M. Ostling, *Adv. Mater.* **2013**, *25*, 3985.
[36] J. Lee, D. H. Kim, J. Y. Kim, B. Yoo, J. W. Chung, J. I. Park, B. L. Lee, J. Y. Jung, J. S. Park, B. Koo, S. Im, J. W. Kim, B. Song, M. H. Jung, J. E. Jang, Y. W. Jin, S. Y. Lee, *Adv. Mater.* **2013**, *25*, 5886.
[37] B. Yoon, D. Y. Ham, O. Yarimaga, H. An, C. W. Lee, J. M. Kim, *Adv. Mater.* **2011**, *23*, 5492.

[38] T. H. J. van Osch, J. Perelaer, A. W. M. de Laat, U. S. Schubert, *Adv. Mater.* **2008**, *20*, 343.
[39] H. H. Lee, K. S. Chou, K. C. Huang, *Nanotechnology* **2005**, *16*, 2436.
[40] L. Li, L. Pan, Z. Ma, K. Yan, W. Cheng, Y. Shi, G. Yu, *Nano Lett.* **2018**, *18*, 3322.
[41] S. Ma, F. Ribeiro, K. Powell, J. Lutian, C. Moller, T. Large, J. Holbery, *ACS Appl. Mater. Interfaces* **2015**, *7*, 21628.
[42] Y. Zhang, N. Anderson, S. Bland, S. Nutt, G. Jursich, S. Joshi, *Sens. Actuators, A* **2017**, *253*, 165.
[43] P. He, J. R. Brent, H. Ding, J. Yang, D. J. Lewis, P. O'Brien, B. Derby, *Nanoscale* **2018**, *10*, 5599.
[44] A. Russo, B. Y. Ahn, J. J. Adams, E. B. Duoss, J. T. Bernhard, J. A. Lewis, *Adv. Mater.* **2011**, *23*, 3426.
[45] X. Liao, Z. Zhang, Q. Liao, Q. Liang, Y. Ou, M. Xu, M. Li, G. Zhang, Y. Zhang, *Nanoscale* **2016**, *8*, 13025.
[46] B. C. Zhang, H. Wang, Y. Zhao, F. Li, X. M. Ou, B. Q. Sun, X. H. Zhang, *Nanoscale* **2016**, *8*, 2123.
[47] X. Zhao, Q. Hua, R. Yu, Y. Zhang, C. Pan, *Adv. Electron. Mater.* **2015**, *1*, 1500142.